Distinguishing prostate cancer from benign confounders via a cascaded classifier on multi-parametric MRI

G.J.S. Litjens[a], R. Elliott[b], N. Shih[c], M. Feldman[c], J.O. Barentsz[a], C.A. Hulsbergen - van de Kaa[a], I. Kovacs[a], H.J. Huisman[a] and A. Madabhushi[b]

[a]Radboud University Nijmegen Medical Centre, Nijmegen, The Netherlands;
[b]Case Western Reserve University, Cleveland, USA;
[c]University of Pennsylvania, Philadelphia, USA;

ABSTRACT

In this paper a new cascaded classifier is introduced to separate prostate cancer and benign confounders on MRI. Specific features to distinguish each of the benign classes will be selected in each step of the cascade, as opposed to a single-shot classifier, which only has the opportunity to learn features common to all confounders, or a multi-class classifier, which tries to learn all distinguishing features at once. Learning how to separate benign confounders from prostate cancer is important because the imaging characteristics of these confounders are poorly understood. The diagnostic uncertainty this causes leads to unnecessary biopsies and overtreatment. We used an annotated prostatectomy data set of 31 patients with multi-parametric MRI to identify specific features for benign prostatic hyperplasia (BPH), high-grade prostatic intraepithilial neoplasia (HGPIN), atrophy and inflammation, which are the most common benign confounders in prostate cancer diagnosis. Using the prostatectomy specimens allowed us to accurately map annotations on the histological slides to the MRI. The prostatectomy slides were carefully co-registered to the corresponding MRI slices using an elastic registration technique. We extracted texture from the T2-weighted imaging, pharmacokinetic features from the dynamic contrast enhanced imaging and diffusion features from the diffusion-weighted imaging for each of the confounder classes and prostate cancer. These types of features were selected because they form the mainstay of clinical diagnosis. Relevant features for each of the classes were selected using maximum relevance minimum redundancy feature selection, because it allows us to select features independent of the classifier used. The selected features were then incorporated in a cascading classifier, which can focus on easier sub-tasks at each stage, leaving the more difficult-to-separate classes for later stages. Results show that distinct features are relevant for each of the benign classes, for example the fraction of extra-vascular, extra-cellular space in a voxel is a clear discriminator for inflammation. Furthermore, the cascaded classifier outperforms both multi-class and one-shot classifiers in overall accuracy: 0.76 versus 0.71 and 0.62.

Keywords: CAD, feature selection, cascading classification, prostate cancer, MRI, confounders

1. INTRODUCTION

One of the most difficult tasks in diagnosing prostate cancer on MRI is separation between prostate cancer and benign confounders like atrophy, inflammation, benign prostatic hyperplasia (BPH) and high-grade prostatic intraepithilial neoplasia (HGPIN).[1,2] One reasons is the widely different image sequences obtained with MRI and the difficulty of mentally combining these images to come to a correct diagnosis. The current PI-RADS standard for reporting MRI does not yet offer guidelines which allow discrimination between specific confounders and prostate cancer.[3] The diagnostic uncertainty caused by the inability to discriminate certain benign diseases from prostate cancer can lead to unnecessary biopsies and thus complications and over-treatment. Improved understanding of the image characteristics of these confounders across the different MRI sequences (T2-weighted (T2w), dynamic contrast enhanced (DCE) and diffusion-weighted (DWI)) might improve the PI-RADS standard and subsequently the detection and diagnosis of prostate cancer.[4] Additionally, the image characteristics can be used to identify features which could increase the performance of computer-aided detection and diagnosis systems for prostate cancer.[5–7]

An illustration of this problem can be found in Figure 1. In Figure 1a we show what happens when we group all confounders as a single class. A linear discriminant classifier is not able to separate the cancer class

from the benign class and as such assigns every sample to the benign class, which is what happens in one-shot classification. In Figure 1b, we show what happens when you use the same features, but only classify atrophy versus cancer. Here the linear discriminant classifier is able to create an accurate decision boundary. Figure 1c-e further illustrate this for the other confounding classes; when picking the right features, the classifier can separate the individual benign confounders from cancer, whereas it cannot when we group them all the confounders together.

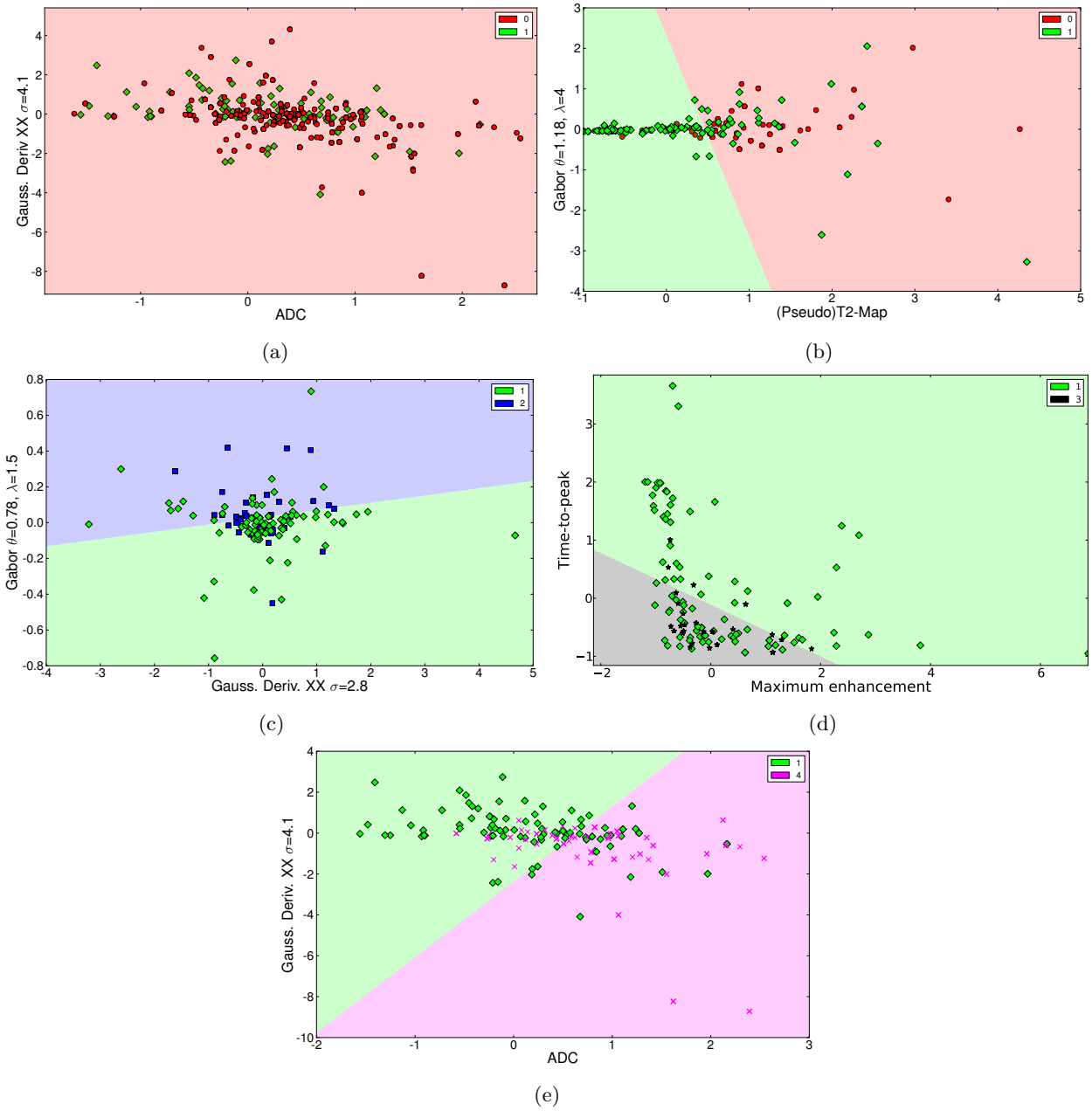

Figure 1: Figure a. shows the results for training an LDA classifier to separate all the benign confounding classes (0) and cancer (1) at once given two features. As it is unable to discriminate the classes, it assigns every sample to class 0. The other figures show that in a cascaded setting, separating out one benign confounder per step, gives a reasonable decision boundary given discriminative features. In figures b-e class 0 is atrophy, class 1 is cancer, class 2 is BPH, class 3 is inflammation and class 4 is HGPIN.

The types of features we use to characterize the benign confounders are based on the diagnostic guidelines presented in.[3] The T2-weighted imaging is mostly used for it's high resolution and contrast, allowing detailed visualization of the tissue anatomy. From clinical guidelines we know that the T2-weighted images are especially useful to assess the texture of prostate lesions.[3] Prostate cancer exhibits a so-called 'erased charcoal sign', a smudge-like dark texture on T2-weighted images.[3] Different benign confounders might also express different types of textures.

Diffusion weighted imaging is specifically useful for characterizing tissue at a microscopic level, enabling us to assess traits like cell density at a macro level. In diffusion weighted imaging, several images with different b-values are acquired. Increasing b-values mean increasing diffusion-weighting. Areas of low diffusivity tend to appear bright on high b-value images. Furthermore, to remove protocol dependency an apparent diffusion coefficient map is calculated, which is a roughly quantitative measure of tissue diffusivity. Prostate cancer has a high cellular density compared to the normal glandular structure of the prostate. This results in a reduced diffusivity in cancerous tissue and thus a high signal in high b-value images and subsequently a low apparent diffusion coefficient values.

Finally, dynamic contrast enhanced MRI result in signal over time curves and shows the uptake of contrast agent in tissue. This allows us to measure attributes of the tissue vasculature, like the relative fraction of extra-vascular, extra-cellular space in each voxel and micro-vessel permeability. Prostate cancer lesions tend to have leaky micro-vasculature, which results in fast initial enhancement and wash-out.

To be able to assess whether these identified features are useful in discriminating the different confounders and cancer, we can integrate them into different classification strategies. Two traditional classification strategies exist to distinguish these benign confounders and prostate cancer. One option is to use a single shot classification approach, considering all the benign confounders as a single class and trying to differentiate this class from prostate cancer. The second option is to use a multi-class classification approach in which each benign confounder is a separate class. In this paper we will also investigate a third strategy: the use of a cascaded classifier to separate the confounding classes and prostate cancer step-by-step. This is more suitable than a regular one-shot classification or a multi-class classification approach because it sub-divides the difficult task of separating confounders and cancer into easier sub-problems, thus circumventing issues with similar classes. Furthermore, it allows us to perform feature selection for each problem separately.

For this paper we obtained a unique MRI/histology data set with annotations of cancer and the benign confounding classes on the histopathologic slides. The prostatectomy slides were then carefully co-registered to the MRI to obtain the MR regions corresponding to the different classes. Texture, pharmacokinetic and intensity features were extracted for each of the classes, after which we used maximum relevance minimum redundancy (mRMR) feature selection[8] to identify the most important features for each class. Using this information a cascading classifier which will remove each confounding class in a step-by-step approach was created. Subsequently, the cascaded classifier was evaluated with respect to accuracy of classifying cancer and compared to single-shot two-class and multi-class classification.

2. PREVIOUS WORK AND NOVEL CONTRIBUTIONS

Only little work has been done on accurately characterizing the appearance of different benign confounders in prostate MRI, most likely due to difficulty of obtaining accurate annotations. Several groups have investigated specific confounding classes using a single modality, for example benign prostatic hyperplasia on diffusion-weighted imaging (Liu et al.,[9] Oto et al.[10]). Another example is the differentiation of prostatitis using diffusion-weighted imaging (Nagel et al.[11]). None of these groups have looked at all the benign confounders or all the modalities.

There has been some previous work on computer-extracted features for the detection of prostate cancer.[6] investigated the use of magnetic resonance spectroscopy in combination with T2-weighted imaging to identify the voxels that are affected by prostate cancer. They also introduced the use of wavelet embedding to map MRS and T2-W texture features into a common space. This work was further expanded and evaluated in.[7] Niaf et al.[12] presented the use of computer-aided diagnosis in the peripheral zone of the prostate using DCE features (similar to Vos et al.[13]). They confirmed the results in discriminating prostate cancer from normal regions (area

under the ROC curve (AUC)=0.89) and discriminating prostate cancer from suspicious benign regions (AUC of 0.82). Lastly, Viswanath et al.[14] investigated the use of texture features to discriminate prostate cancer from normal and benign regions. He also found different texture features were important depending on the originating prostatic zone of the cancer.

In this paper we have several novel contributions:

1. Use of pathology annotated benign confounder classes to identify corresponding regions on the MRI
2. Identifying important imaging features per confounding class over all prostate MRI parameters
3. Improving computerized prostate cancer diagnosis using a cascaded classifier which incorporates per-stage feature selection

3. METHODOLOGY

Annotation and co-registration of histopathology

A pathologist contoured distinct examples of each benign confounding class and prostate cancer on the histopathology slides using the Aperio ImageScope software, if present. The pathology annotations were transferred to the MRI by registering the whole-mount slide using a thin plate spline registration technique.[14] The process, in a step-by-step fashion, goes as follows:

1. The slice in the MRI which corresponds to the prostatectomy slide is established by an image analysis researcher under the supervision of a radiologist by comparing landmarks on the pathology and the MRI.
2. Corresponding points are indicated on the prostate boundary for both the prostatectomy slide and the MRI slice.
3. A b-spline transformation is calculated to move from the prostatectomy coordinate space to MRI coordinate space.
4. The histopathology image is transformed to the MRI space using this b-spline transformation. A visual assessment whether the registration is accurate is made.
5. The annotations of the pathologist are morphed to the MRI using this b-spline transformation.

Features and feature selection

3.0.1 Correction of intensity drift

Intensity drift is an issue that is well known in MRI.[14] This means that intensities differ from scanner to scanner and even from protocol to protocol on the same scanner. To circumvent this issue in T2-weighted images we can calculate a (pseudo)T2-map using the transverse T2W-image and the proton density-weighted image as described in.[15] This approach uses MR signal equations and a muscle reference region of interest to reduce intensity drift between the different studies.

3.0.2 T2-weighted imaging

For the T2-weighted texture features we calculated several often used filter types: 13 Haralick texture features using 3 kernel sizes (3,5 and 7 voxels), Gabor texture features using 4 different angles and 3 different wavelengths between 1mm and 6mm and Gaussian derivatives up to second order using 4 different scales between 1mm and 6mm.[14] The texture features were all calculated on the (pseudo)T2-map.

Diffusion-weighted imaging

From the diffusion-weighted imaging we directly incorporate the apparent diffusion coefficient and b800 image. Furthermore, as prostate cancer lesions tend to have a focal appearance on diffusion weighted imaging, we implemented the multi-scale blobness filter proposed by Li et al.[16] and calculated the filter using 4 scales between 1 and 6 mm on the b800 and ADC images.

Category	Feature name	MR sequence	Feature settings
Intensity	(Pseudo)T2-map[19] ADC b-800	T2W DWI DWI	
Texture	2D Multi-scale Gaussian Derivatives[19] 2D Haralick texture measures[14] 2D Multi-angle Gabor[14] 2D Li Multi-scale blobness[16]	T2Map T2Map T2Map T2Map, ADC, b800, Ktrans, Kep, Ve, time-to-peak, maximum enhancement, wash-out rate	Up to 2nd order, σ=2.0, 2.67, 4.1 and 6.0 mm Kernel sizes 3, 5, 7 voxels Four angles: 0, $\frac{\pi}{4}$, $\frac{\pi}{2}$, $\frac{3\pi}{4}$, λ=1.5, 2 and 4 voxels σ= 2.0, 2.67, 4.1 and 6
Pharmacokinetic	Curve fitting parameters[5] Std. Tofts PK model[5]	DCE DCE	Time-to-peak, maximum enhancement, wash-out rate Ktrans, Kep, Ve

Table 1: Table of feature and feature settings calculated on the different MR sequences and used in the different classifiers

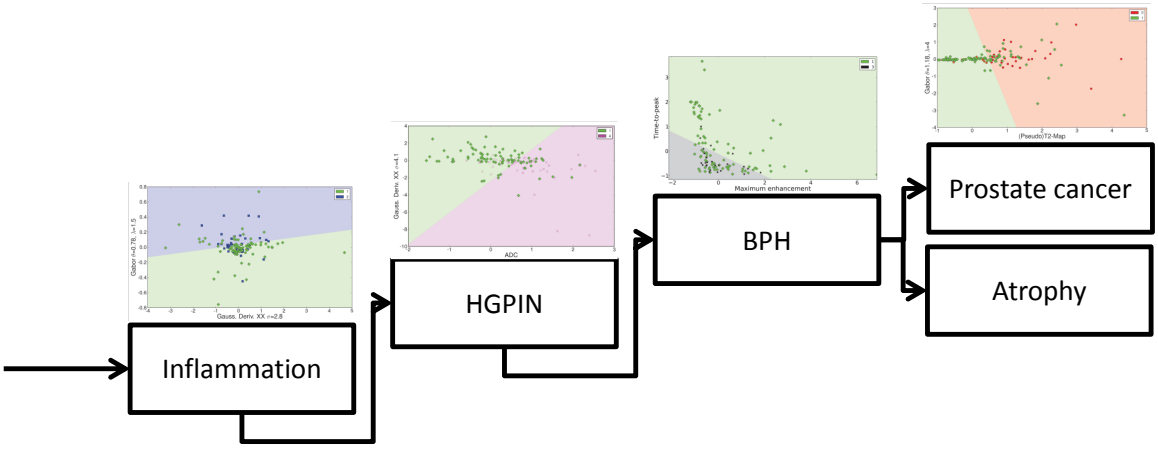

Figure 2: Schematic representation of the cascade classification strategy

Dynamic contrast-enhanced imaging

Dynamic contrast-enhanced MRI also tends to suffer from scanner and protocol dependency. To remove this dependency and extract the most useful information from these curves we implemented curve fitting and pharmacokinetic modeling routines as presented in[17,18] and.[5] The temporal resolution of the DCE time series was 4 seconds. To capture characteristics on the micro-vasculature we included total of 3 curve features (time-to-peak, washout rate and maximum enhancement)[18] and 3 pharmacokinetic features (Ktrans, Kep, Ve).[5] Furthermore, as cancer also tends to have a focal appearance on DCE MRI we also calculate the Li blobness filter on the Ktrans, Kep, Ve, maximum enhancement, time-to-peak and wash-out rate images.

Feature selection

The maximum relevance, minimum redundancy (mRMR) feature selection technique[8] was used to determine features for each of the confounding classes by splitting the data into four different sets, each representing a two-class classification task (BPH vs. cancer, inflammation vs. cancer, HGPIN vs. cancer and atrophy vs. cancer). This mRMR feature selection tries to maximize the mutual information between the individual features and the class labels and minimize the mutual information between features to select the most relevant features without redundancy. After mRMR feature selection, unique features discriminating each benign class from cancer were identified. mRMR feature selection was selected because it tends to give good results at reasonable computation time and does not need parameter optimization or nested cross-validation loops like for example sparse coding or sequential forward floating feature selection.

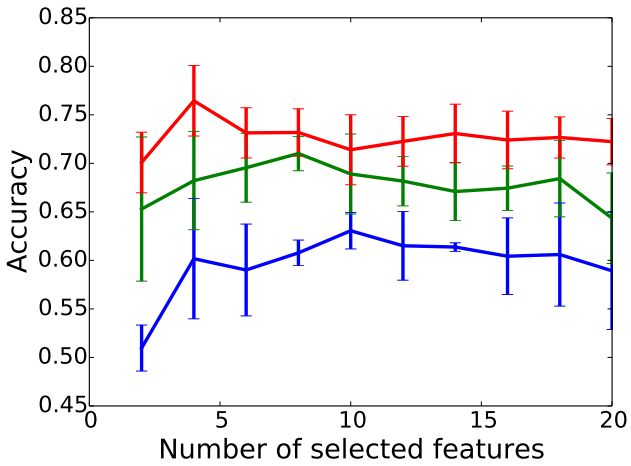

Figure 3: Two-class accuracies over the number of selected features for the simple two-class strategy (green), multi-class classification (blue) and the cascade classification (red) including 95% confidence intervals

Rank	Inflammation	BPH
1	Ve	Gauss. Deriv ($o = yy$, $\sigma = 4.1$)
2	Haralick Sum Variance (w=7)	b800 intensity
3	Blobness ADC	Time-to-peak
4	Gauss. Deriv ($o = xx$, $\sigma = 4.1$)	Blobness ADC
5	Max. Enhancement	Gabor ($\lambda = 1.5$, $\theta = 0.0$)
Rank	**Atrophy**	**HGPIN**
1	Gauss. Deriv ($o = -$, $\sigma = 2.8$)	Gauss. Deriv ($o = xx$, $\sigma = 4.1$)
2	Haralick Measure of Correlation1 (w=3)	Blobness b800
3	Blobness (Pseudo)T2Map	ADC intensity
4	Blobness Kep	Haralick Contrast (w=3)
5	Gabor ($\lambda = 2.0$, $\theta = 0.0$)	Blobness time-to-peak

Table 2: Selected features for each of the benign classes, unique features are indicated with gray backgrounds

Cascading classifier

The feature selection step can be used to improve the classification of unknown samples in prostate cancer and benign disease by using a cascading classification scheme. At the start of the cascade the potential labels for a sample consists of all benign confounder classes and prostate cancer. At each step of the cascade the classifier attempts to separate out one type of benign disease. This is schematically shown in Figure 2. The order of the cascade was empirically determined, however the end result was relatively robust to the order of cascade. At each step of the cascade mRMR feature selection is used. Training data at that step consists of the benign confounder to be detected at that stage (in step 1 inflammation), which is given class label 0 and all classes that are upstream in the cascade (given class label 1). The training folds were balanced before feature selection. A linear discriminant classifier is then trained with the selected features. In each step either a sample is identified as the desired benign class and removed from further classification, or it moves on to the next stage. At the final stage the remaining samples are either classified as atrophy or as prostate cancer.

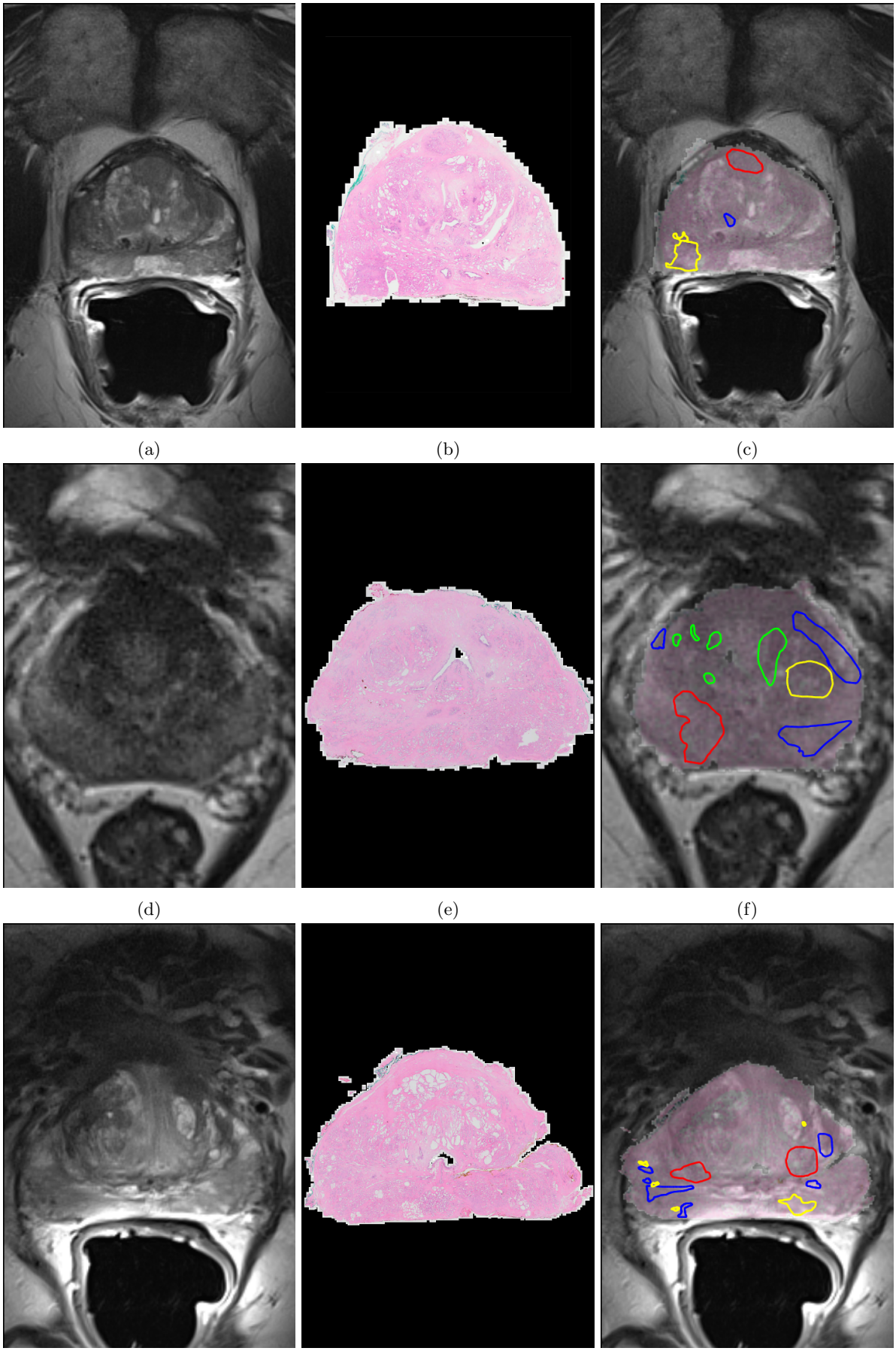

Figure 4: Example images of an T2-weighted MRI (a,d,g) and a H&E stained prostatectomy slide (b,e,h) and the result of the subsequent MRI/histology registration with (c,f,i) annotations. In this example prostate cancer is indicated in yellow, a BPH nodule in red, inflammation in blue and atrophy in green.

4. EXPERIMENTAL RESULTS AND DISCUSSION

Patient data, annotation and co-registration

For this study we included 31 patients with an MRI including T2-weighted, dynamic contrast-enhanced, diffusion-weighted and proton density-weighted image sequences. After prostatectomy, in total 44 histological H&E stained slides where digitized, with at least 1 slide per patient. The slides selected contained the largest tumor volume, based on the interpretation by an experienced pathologist. Areas of prostate cancer, BPH, atrophy, inflammation and HGPIN were subsequently annotated on each slide by one of two pathologists. The annotations made on the histopathologic slides where transferred to the MRI using the methodology explained in subsection 3. This resulted in a total of 68 atrophy, 25 BPH, 58 PIN, 47 inflammation and 93 prostate cancer lesions. An example of co-registered annotations is shown in Figure 4.

Feature selection results

In Table 2, the top 5 selected features for each of the different benign vs. cancer classification tasks are presented. Each task has a number of distinct unique features (indicated with the gray background). We also show the top 2 selected features in Table 3. We can see that all confounders have at least 3 unique features. These selected features also have a physiological meaning, for example inflammation often results in marked vascular changes like increased blood flow and permeability (to allow leukocytes to move to the inflamed tissue) and increased extra-cellular, extra-vascular space due to dying (apoptotic or necrotic) cells. From Table 2 we can see that this has been picked up by the feature selection strategy (selected features 1 and 5, Ve and maximum enhancement) and that these features can help discriminate between inflammation and prostate cancer.

Another example is the feature selected for atrophy. Atrophy of the prostate results in a loss of the regular structure of the glands in the prostate (reduced infolding, cytoplasm volume and presence of corpora amylacea). Atrophy tends to be focal and looks texturally different from prostate cancer on pathology. This can also be recovered on the MRI if we look at Table 2, where 3 out of the top 5 features are related to texture. Finally, an excellent discriminator of atrophy versus prostate cancer would be the blobness feature on the (pseudo)T2-map, as prostate cancer tends to have a diffuse appearance with irregular border, whereas the focal appearance of atrophy on pathology carries over to the T2-weighted MRI.

Classification results

Next to the top 2 selected features a likelihood map for cancer detection in a confounder vs. cancer setting in for both the single-shot classifier and the cascaded classifier was also added to Figure 3. The validation of the cascaded classifier was performed in a five-fold patient-based cross-validation (20 repeated runs). The evaluation is based on the overall accuracy in separating benign disease and prostate cancer on a lesion level and compared to direct two-class classification of benign disease and prostate cancer and multi-class classification with and without feature selection. In the multi-class classification the resulting benign classes are grouped as one benign class after classification. The amount of features was varied between 2 and 20 in steps of 2. The results are shown in Figure 3. The cascaded classifier outperforms the single-shot classifier and the multi-class classifier in the overall accuracy of correctly classifying voxels as either containing cancer or not containing cancer. The overall maximum accuracy is 76.4% when using 4 features for the cascading classifier and 63.0% and 71.0% for the single-shot classification and the multi-class classifier at 10 and 8 features respectively. Overall accuracy is limited because some lesions annotated on pathology ended up being only a couple of voxels on the MRI and are indistinguishable from normal tissue.

5. CONCLUDING REMARKS AND CONTRIBUTIONS

A major issue in prostate MRI is the presence of confounding benign classes which share image characteristics with prostate cancer. By improving the understanding of specific imaging characteristics of benign confounders potentially the diagnosis of prostate cancer can be improved.

We presented a co-registration technique combining pathology and MRI to map annotations of these confounders to the MRI. This allowed us to identify features which might help in discriminating between specific confounders and prostate cancer. Furthermore, we combined mRMR feature selection with a cascaded classifier,

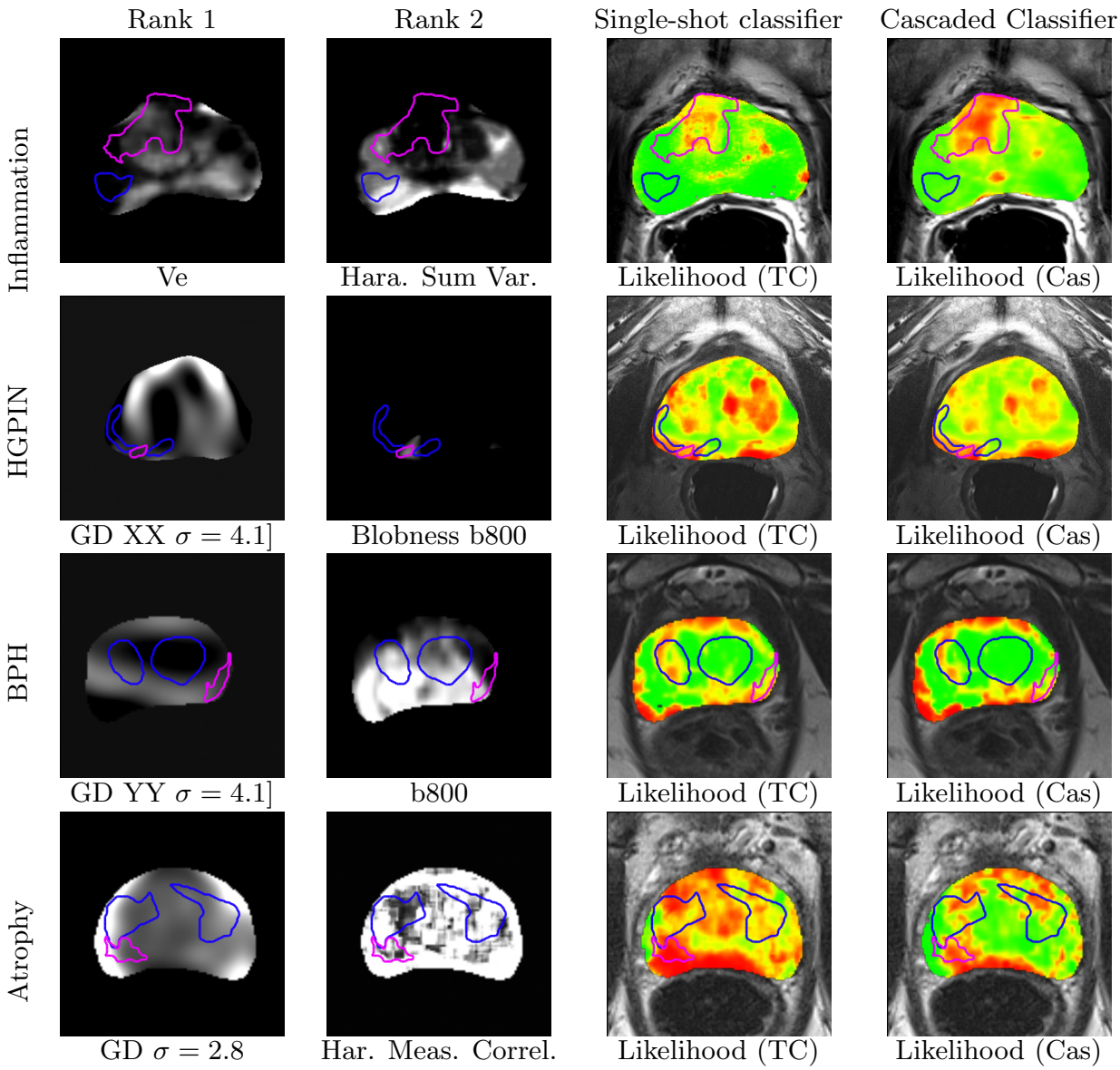

Table 3: The top 2 selected features are shown in the first two columns for each of the benign class versus cancer classification tasks. Each row is a separate patient. The last two columns show likelihood maps for the single-shot classification (column 3) and the cascaded classification (column 4). The overlays indicate likelihood value: transparent, green and red are a zero, low and high value respectively between 0 and 1. The confounding class is indicated with a dark blue contour and prostate cancer with a purple contour. The feature names can be looked up in Table 2

which can step-by-step learn features for each of the confounders, thus simplifying the classification task for the following steps, as opposed to single-shot or multi-class classifiers, which are restricted to only learning features common to all benign classes or having to learn all features at once.

The main results include a top 5 selected features for each of the benign classes, which is found in Table 2. These selected features can be related to the underlying pathology to achieve a better understanding of which pathological processes cause certain image characteristics on MRI. An example here is the fraction of extra-cellular, extra-vascular space, Ve, which is discriminative for inflammation. The results in Tables 3,2 and Figure 3 indicate that to accurately discriminate between the different benign confounder and prostate cancer very specific features are needed. Our classification results also show improved accuracy in classifying cancer versus benign disease when using a cascading approach as opposed to a single-shot or multi-class classifier.

This study also has some limitations. We did not discriminate on lesion size when converting the pathology annotations to the MRI. This resulted in some very small lesions (< 5 voxels) which might get misclassified due to issues like partial volume effect or small co-registration errors. We also did not take into account combined classes, i.e. sometimes areas of atrophy or cancer also show active inflammation.

In the future we would like to validate our approach on a larger cohort and experiment with more complex classifiers for each of the steps in the cascade. Furthermore, we would like to look into a soft per-class classification to take into account class overlap (e.g. inflammation occurring together with atrophy). Another open question pertains to which feature selection strategy works best in combination with a cascaded classifier.

REFERENCES

[1] Hoeks, C. M. A., Hambrock, T., Yakar, D., Hulsbergen-van de Kaa, C. A., Feuth, T., Witjes, J. A., Fütterer, J. J., and Barentsz, J. O., "Transition zone prostate cancer: Detection and localization with 3-t multiparametric MR imaging," *Radiology* **266**, 207–217 (2013).

[2] Bratan, F., Niaf, E., Melodelima, C., Chesnais, A. L., Souchon, R., Mège-Lechevallier, F., Colombel, M., and Rouvière, O., "Influence of imaging and histological factors on prostate cancer detection and localisation on multiparametric MRI: a prospective study," *Eur Radiol* , 1–11 (2013).

[3] Barentsz, J. O., Richenberg, J., Clements, R., Choyke, P., Verma, S., Villeirs, G., Rouviere, O., Logager, V., Fütterer, J. J., and European Society of Urogenital Radiology, "ESUR prostate MR guidelines 2012," *Eur Radiol* **22**, 746–757 (2012).

[4] Lovett, K., Rifkin, M. D., McCue, P. A., and Choi, H., "MR imaging characteristics of noncancerous lesions of the prostate," *J Magn Reson Imaging* **2**, 35–39 (1992).

[5] Vos, P. C., Barentsz, J. O., Karssemeijer, N., and Huisman, H. J., "Automatic computer-aided detection of prostate cancer based on multiparametric magnetic resonance image analysis," *Phys Med Biol* **57**, 1527–1542 (2012).

[6] Tiwari, P., Viswanath, S., Kurhanewicz, J., Sridhar, A., and Madabhushi, A., "Multimodal wavelet embedding representation for data combination (maweric): integrating magnetic resonance imaging and spectroscopy for prostate cancer detection," *NMR Biomed* (2011).

[7] Tiwari, P., Kurhanewicz, J., and Madabhushi, A., "Multi-kernel graph embedding for detection, gleason grading of prostate cancer via MRI/mrs," *Med Image Anal* **17**, 219–235 (2013).

[8] Peng, H., Long, F., and Ding, C., "Feature selection based on mutual information criteria of max-dependency, max-relevance, and min-redundancy," *IEEE Trans Pattern Anal Mach Intell* **27**, 1226–1238 (2005).

[9] Liu, X., Zhou, L., Peng, W., Wang, C., and Wang, H., "Differentiation of central gland prostate cancer from benign prostatic hyperplasia using monoexponential and biexponential diffusion-weighted imaging," *Magn Reson Imaging* **31**, 1318–1324 (2013).

[10] Oto, A., Kayhan, A., Jiang, Y., Tretiakova, M., Yang, C., Antic, T., Dahi, F., Shalhav, A. L., Karczmar, G., and Stadler, W. M., "Prostate cancer: differentiation of central gland cancer from benign prostatic hyperplasia by using diffusion-weighted and dynamic contrast-enhanced MR imaging," *Radiology* **257**, 715–723 (2010).

[11] Nagel, K. N. A., Schouten, M. G., Hambrock, T., Litjens, G. J. S., Hoeks, C. M. A., Haken, B. T., Barentsz, J. O., and Fütterer, J. J., "Differentiation of prostatitis and prostate cancer by using diffusion-weighted MR imaging and MR-guided biopsy at 3 t," *Radiology* **267**, 164–172 (2013).

[12] Niaf, E., Rouvière, O., Mège-Lechevallier, F., Bratan, F., and Lartizien, C., "Computer-aided diagnosis of prostate cancer in the peripheral zone using multiparametric MRI," *Phys Med Biol* **57**, 3833 (2012).

[13] Vos, P. C., Hambrock, T., Barentsz, J. O., and Huisman, H. J., "Computer-assisted analysis of peripheral zone prostate lesions using T2-weighted and dynamic contrast enhanced T1-weighted MRI," *Phys Med Biol* **55**, 1719–1734 (2010).

[14] Viswanath, S. E., Bloch, N. B., Chappelow, J. C., Toth, R., Rofsky, N. M., Genega, E. M., Lenkinski, R. E., and Madabhushi, A., "Central gland and peripheral zone prostate tumors have significantly different quantitative imaging signatures on 3 tesla endorectal, in vivo T2-weighted MR imagery," *J Magn Reson Imaging* **36**, 213–224 (2012).

[15] Litjens, G., Barentsz, J., Karssemeijer, N., and Huisman, H., "Automated computer-aided detection of prostate cancer in MR images: from a whole-organ to a zone-based approach," in [*Medical Imaging*], *Proceedings of the SPIE* **8315**, 83150G–83150G–6 (2012).

[16] Li, B., Christensen, G. E., Hoffman, E. A., McLennan, G., and Reinhardt, J. M., "Establishing a normative atlas of the human lung: Intersubject warping and registration of volumetric CT images," *Acad Radiol* **10**, 255–265 (2003).

[17] Tofts, P. S., Brix, G., Buckley, D. L., Evelhoch, J. L., Henderson, E., Knopp, M. V., Larsson, H. B., Lee, T. Y., Mayr, N. A., Parker, G. J., Port, R. E., Taylor, J., and Weisskoff, R. M., "Estimating kinetic parameters from dynamic contrast-enhanced t(1)-weighted MRI of a diffusable tracer: standardized quantities and symbols," *J Magn Reson Imaging* **10**, 223–232 (1999).

[18] Huisman, H. J., Engelbrecht, M. R., and Barentsz, J. O., "Accurate estimation of pharmacokinetic contrast-enhanced dynamic MRI parameters of the prostate," *J Magn Reson Imaging* **13**, 607–614 (2001).

[19] Litjens, G. J. S., Debats, O. A., van de Ven, W. J. M., Karssemeijer, N., and Huisman, H. J., "A pattern recognition approach to zonal segmentation of the prostate on MRI," in [*Med Image Comput Comput Assist Interv*], *Lect Notes Comput Sci* **7511**, 413–420 (2012).